Paramagnetic Resonance of F Centers in Alkali Halides*

W. C. Holton† AND H. Blum

Physics Department, University of Illinois, Urbana, Illinois

(Received June 30, 1961; revised manuscript received September 18, 1961)

The F-center slow- and fast-passage electron spin resonance has been observed in LiF, LiCl, NaF, NaCl, NaBr, KCl, and KBr. The hyperfine coupling of the F electron to nuclei neighboring the negative-ion vacancy has been measured by electron-nuclear double resonance. Root second moments of the resonance absorption, obtained from slow passage, agree with values calculated from the hyperfine constants. In the case of LiF, the partially resolved structure existing on the slow passage resonance line is shown conclusively to arise from the F center. These experimental results, together with those of previous workers, are compared with the theory of Gourary and Adrian.

I. INTRODUCTION

WITHIN the last two decades there has been a revived interest in the study of alkali halide crystals in which defects are produced either by introducing a stoichiometric excess of one of the constituents or by exposing the crystal to ionizing radiation. Of the defects which may be produced in this manner, the most thoroughly studied has been the F center, whose optical absorption bands in the various alkali halides have been known for some time.[1,2] Since de Boer's[3] original proposal in 1937 that the F center was an electron trapped at a negative-ion vacancy within the crystal, and thus should exhibit paramagnetism, it has been shown through electron spin resonance experiments that the F center is paramagnetic.[4] An unusually broad resonance line (with partially resolved structure in the case of LiF and NaF) has been observed with a g value slightly less than the free-electron g value.[5–10] Assuming the de Boer model, the slight g shift was explained as arising from a spin-orbit interaction between the electron spin moment and the magnetic field due to its orbital motion, while the unusual breadth was attributed to a hyperfine coupling of the electron with the neighboring nuclei, thus inhomogeneously broadening the resonance line. Through the discovery of the electron-nuclear double resonance (ENDOR) technique, Feher[11,12] was later able to prove the correctness of the interpretation given to the observed resonances, and to determine the hyperfine coupling of the F electron to the neighboring

nuclei for F centers in KCl. Since this work, F centers in LiF have also been investigated by ENDOR.[13] The partially resolved 35-line hyperfine structure existing on the broad resonance line for the [111] crystal axis parallel to the external magnetic field, was shown to be consistent with the hyperfine splitting constants obtained from ENDOR experiments.[14]

Based on the de Boer model, several theoretical treatments of the F center have been proposed.[15–18] The more successful theories take account of the atomic structure of the crystal as opposed to a continuum or semi-continuum approach. Kojima[15] and Gourary and Adrian[16] have used the atomistic viewpoint. Kojima has determined the wave function and the energy levels for the F electron in LiF both by the linear combination of atomic orbitals method and by a variational calculation. Gourary and Adrian (GA) have developed a method which is based on a variational calculation, where the potential used is that of a point-ion lattice. Ground and excited state F-electron envelope functions are determined for several of the alkali halides. Expressions are developed for the optical transition energy, the g shift, and the isotropic and anisotropic hyperfine constants. The F-center optical transition energies predicted by the theory are in fair agreement with experimental values and with Ivey's law, which states a relationship between the wavelength of the peak of the F-center optical absorption band and the lattice constant. The predicted g shifts, which are always negative with respect to the free-electron g value and increase in magnitude for the heavier alkali halides are in qualitative agreement with experimental results. There is fair agreement between the theoretical and experimental hyperfine constants.

This paper (1) reports the results of ENDOR, fast-passage, and slow-passage electron spin resonance (ESR) experiments performed at 1.3°K on F centers

[1] F. Seitz, Revs. Modern Phys. 26, 7 (1954).
[2] H. Pick, Suppl. Nuovo cimento 7, No. 2, 498 (1958).
[3] J. H. de Boer, Rec. trav. chim. 56, 301 (1937).
[4] C. A. Hutchinson, Phys. Rev. 75, 1769 (1949).
[5] C. A. Hutchinson and G. A. Noble, Phys. Rev. 87, 1125 (1952).
[6] A. F. Kip, C. Kittel, R. A. Levy, and A. M. Portis, Phys. Rev. 91, 1066 (1953).
[7] G. A. Noble, Bull. Am. Phys. Soc. 3, 178 (1958).
[8] N. W. Lord, quoted by B. S. Gourary and F. J. Adrian, in *Solid-State Physics*, edited by F. Seitz and D. Turnbull (Academic Press, Inc., New York, 1960), Vol. 10, p. 143.
[9] N. W. Lord, Phys. Rev. 105, 756 (1957).
[10] N. W. Lord and C. K. Jen, Bull. Am. Phys. Soc. 1, 12 (1956).
[11] G. Feher, Phys. Rev. 105, 1122 (1957).
[12] W. E. Blumberg and G. Feher, Bull. Am. Phys. Soc. 5, 183 (1960).

[13] N. W. Lord, Phys. Rev. Letters 1, 170 (1958).
[14] W. C. Holton, H. Blum, and C. P. Slichter, Phys. Rev. Letters 5, 197 (1960).
[15] T. Kojima, J. Phys. Soc. Japan 12, 908 (1957) and 12, 918 (1957).
[16] B. S. Gourary and F. J. Adrian, in *Solid-State Physics*, edited by F. Seitz and D. Turnbull (Academic Press, Inc., New York, 1960), Vol. 10, p. 127.
[17] D. L. Dexter, Phys. Rev. 93, 244 (1954).
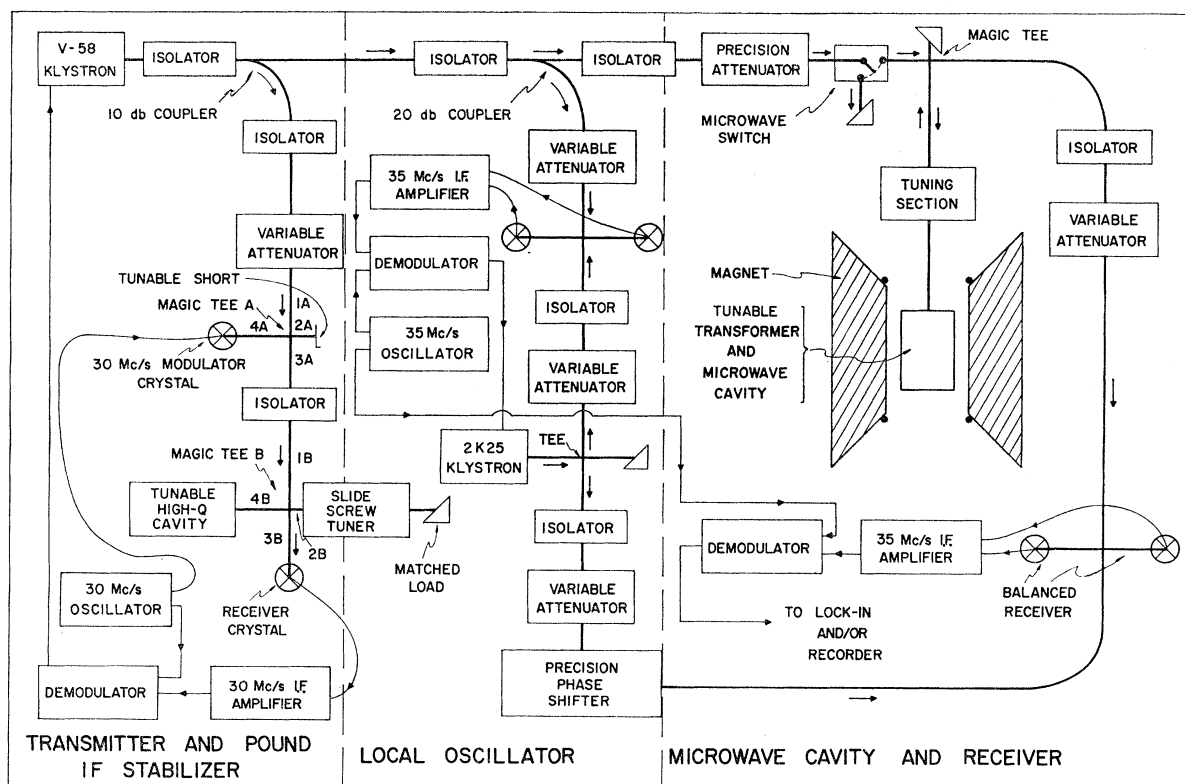[18] J. A. Krumhansl, Phys. Rev. 93, 245 (1954).

FIG. 1. Block diagram of spectrometer.

in LiF, LiCl, NaF, NaCl, NaBr, KCl, and KBr; (2) compares these results, together with the results of previous workers,[19-24] with the Gourary and Adrian theory; and (3) presents conclusive proof that the structure existing on the slow passage electron spin resonance line of x-rayed LiF crystals arises from the F center.

Section II contains a description of the X-band microwave paramagnetic resonance spectrometer and presents the details of the thick-wall ENDOR microwave cavity used in these experiments. The theory necessary for comparison of theory with experiment is presented in Sec. III. The experimental procedure and results for each of the crystals investigated are contained in Sec. IV. A comparison of the results with the GA theory is made in Sec. V.

II. APPARATUS

The X-band microwave paramagnetic resonance spectrometer is a high-sensitivity superheterodyne

system,[25] which employs a modified Pound intermediate frequency stabilization scheme for the transmitter klystron, a phase-locked local oscillator klystron, a separate sample cavity bridge, and a balanced mixer receiver.

A block diagram of the system is shown in Fig. 1. The transmitter klystron is stabilized to approximately 2.5 parts in 10^8 or 250 cycles/sec jitter noise on a tunable high-Q ($Q=110\,000$) cavity. A separate klystron (local oscillator) is used to provide reference power to the balanced mixer receiver. The local oscillator klystron's beat note with the transmitter klystron is phase detected against a 35-Mc/sec crystal oscillator, the detected signal controlling the local oscillator frequency; thus, the local oscillator automatically tracks the transmitter, and the intermediate frequency of the receiver is 35 Mc/sec. The balanced crystal mixer receiver sees power reflected from the sample cavity, which is operated "matched" to the line.

There are three distinct virtues of this spectrometer design in addition to increased sensitivity: (1) The receiver can detect either the real or the imaginary part of the signal reflected from the sample cavity independent of the "degree of match" of the sample cavity, and thus independent of the power incident on the sample, without a rebalancing of the system; (2) the system has low noise for measuring dispersion,

[19] Y. W. Kim, R. Kaplan, and P. J. Bray, Bull. Am. Phys. Soc. 3, 178 (1958).
[20] Y. W. Kim, R. Kaplan, and P. J. Bray, Bull. Am. Phys. Soc. 4, 261 (1959).
[21] G. J. Wolga and M. W. P. Strandberg, J. Phys. Chem. Solids 9, 309 (1959).
[22] R. T. Schumacher (private communication).
[23] J. S. Hyde, Mass. Inst. Technol. Lab. for Ins. Res. Tech. Rep. 142 (1959); Phys. Rev. 119, 1483 (1960).
[24] H. C. Wolf and K. H. Hausser, Naturwissenschaften 23, 1 (1959).
[25] G. Feher, Bell System Tech. J. 36, 449 (1957).

in contrast to systems which "lock" the transmitter klystron to the sample cavity; and (3) the system has a fast response (bandwidth of the i.f. amplifier) as compared to bolometer systems that have an upper frequency limit of approximately 1 kc/sec. A disadvantage of this design is that the klystron frequency may slowly drift from the resonant frequency of the sample cavity, unbalancing the system.

A sufficiently fast mechanical pumping system with associated low-temperature Dewars is provided so that the sample and microwave cavity may be maintained at 1.3°K. The inside of the waveguide and the sample cavity are filled with Styrofoam so that liquid helium is excluded from the major volume of the cavity. As shown in Fig. 2, the sample is located midway on the narrow side wall of the TE_{101} mode cavity which is slit vertically on the center line of the broad face and across the two ends, separating the cavity into two pieces. The two cavity halves are electrically insulated from the waveguide and from each other by one-mil Mylar, and a radio-frequency coil of from four to eight turns wound on the outside with a 10-mil spacing away from the outside cavity walls. This assembly is held rigidly against the microwave transformer tuning section by the separate bottom plate. The rf power is provided by a swept-frequency oscillator using a 3E29 power tetrode.

With this design, leakage of microwave power from the cavity is sufficiently low that it does not contribute to the noise of the spectrometer; while, at the same time, excellent rf penetration into the cavity from the rf coil is achieved. Low microwave power leakage is obtained by accurate machining of the cavity and by the thick conducting walls (thickness=0.050 in.), which also suppress microphonic vibrations and breathing of the cavity walls at the magnetic field modulation frequency. The rf field at the sample arises from surface current on the interior cavity walls of each cavity half. This current is decreased by the shunting effect of displacement current between the two cavity halves. Thus, the thick walls do not shield the rf field from the sample as long as the inductive impedance of one cavity half is small compared to the capacitive impedance between the two cavity halves. This design has been found to be effective up to 80 Mc/sec.

III. THEORY

The electron spin resonance spectra of F centers in alkali halides is adequately described by a spin Hamiltonian which assumes that the electronic spectroscopic splitting factor (g) is isotropic, and that the hyperfine interaction of the electron trapped at the negative ion vacancy with each neighboring nucleus is axially symmetric about a line which joins the negative ion vacancy to that nucleus. Axial symmetry is assured by a nondistorted crystal symmetry only for those nuclei which lie along either a [100] or a [111] crystal axis. However,
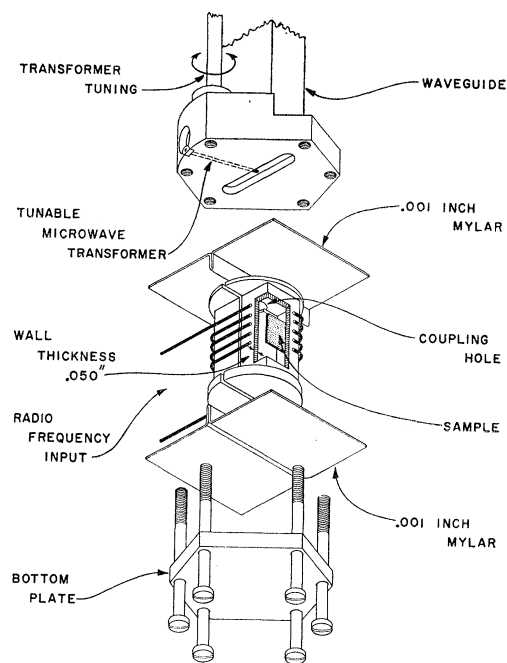

FIG. 2. Microwave cavity design.

axial symmetry with respect to the hyperfine interaction has been found to be a good approximation for all nuclei. The electron spin is quantized along the direction of the external magnetic field, while the nuclear spin is properly quantized along the direction of an effective magnetic field arising from the electron magnetic moment and the external field. However, this effective field direction is nearly parallel to the external field direction for each of the two cases which arise: (1) The isotropic hyperfine energy is greater than the nuclear Zeeman energy while the anisotropic hyperfine energy is small compared to the isotropic hyperfine energy; (2) the nuclear Zeeman energy is large compared to the hyperfine energy. The first case arises for those nuclei nearest and next-nearest to the negative-ion vacancy where the F-electron density is large, while the second case arises for the nuclei further removed from the vacancy.

In the approximation that the nuclear spins may be quantized along the external field direction, the nuclear and electron transition frequencies corresponding to $\Delta M_{I_\alpha} = \pm 1$ and $\Delta M_s = \pm 1$ are given from a first-order perturbation calculation, respectively, by

$$h\nu_\alpha = \pm (\mu_\alpha/I_\alpha)H_0 + \tfrac{1}{2}a_\alpha + \tfrac{1}{2}b_\alpha(3\cos^2\theta_\alpha - 1)$$
$$+ Q_\alpha'(3\cos^2\theta_\alpha - 1)(M_\alpha - \tfrac{1}{2}), \quad (1)$$

$$h\nu_e = g\beta_0 H_0 + \sum_\alpha [a_\alpha + b_\alpha(3\cos^2\theta_\alpha - 1)]M_{I_\alpha}, \quad (2)$$

where θ_α is the angle between the external magnetic field (H_0) and the axis of symmetry passing through the α nucleus, M_α is the higher value in the $\Delta M_{I_\alpha} = \pm 1$ transition μ_α is the magnetic moment of the α nucleus, g is the electronic spectroscopic splitting factor, β_0 is

the electronic Bohr magneton, and where a_α, b_α, and Q_α' are given by

$$a_\alpha = \frac{16\pi}{3}\left(\frac{\beta_0\mu_\alpha}{I_\alpha}\right)|\Phi_F(\alpha)|^2, \tag{3}$$

$$b_\alpha = \frac{\beta_0\mu_\alpha}{I_\alpha}\left\langle\frac{3\cos^2\theta_{\alpha F}-1}{r_{\alpha F}^3}\right\rangle_{av}, \tag{4}$$

$$Q_\alpha' = \frac{3eQ_\alpha}{4I_\alpha(I_\alpha-1)}(\partial^2 V/\partial z^2)_\alpha, \tag{5}$$

where $\Phi_F(\alpha)$ is the F-electron wave function evaluated at the αth lattice site, and Q_α is the electric quadrupole moment of the αth nucleus. V is the crystalline electric field potential, $\mathbf{r}_{\alpha F}$ is the position vector of the F electron measured with α as the origin, and $\theta_{\alpha F}$ is the angle between the electron position $\mathbf{r}_{\alpha F}$ and the symmetry axis. Castner and Känzig present the details of this type of perturbation treatment as applied to the V_k center.[26]

A. ENDOR

In an ENDOR experiment the external field, the field modulation, the microwave field, and the microwave frequency are adjusted so that a portion of the
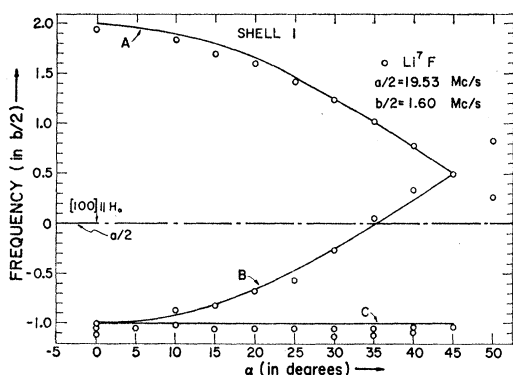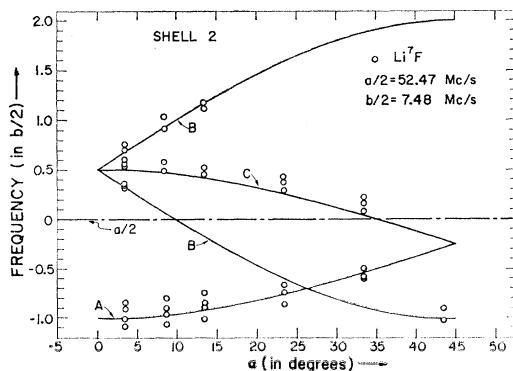

FIG. 3. Shell 1.

FIG. 4. Shell 2.

[26] T. G. Castner and W. Kanzig, J. Phys. Chem. Solids 3, 178 (1957).
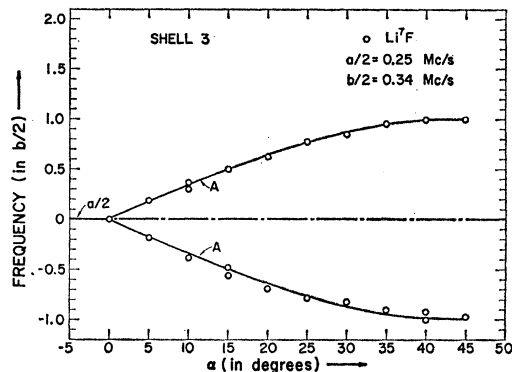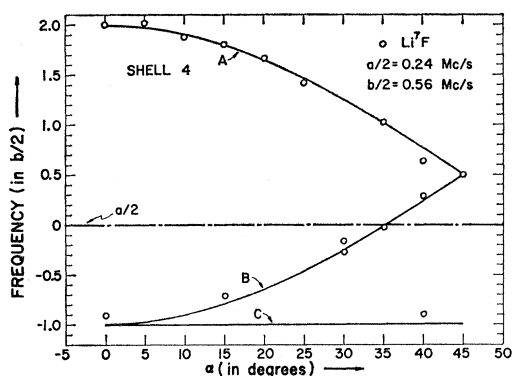

FIG. 5. Shell 3.

FIG. 6. Shell 4.

inhomogeneously broadened resonance is partially saturated. This situation, called "hole eating" in the line, is maintained in steady state. Additional rf power is then applied to excite $\Delta M_I = \pm 1$ transitions, which are detected by observing a change in the electron resonance from the established steady-state condition. By this technique the resolution obtainable is increased by several orders of magnitude over that for the usual slow passage electron spin resonance conditions. Thus, the isotropic, anisotropic, and quadrupole couplings can be determined while they are unresolved in slow or fast passage.

The ENDOR signals can be grouped, each group arising from a shell of nuclear sites which are crystallographically equivalent with respect to the F-center negative-ion vacancy, and whose distance from the vacancy is $N^{\frac{1}{2}}$ times the lattice parameter, where N is an integer. A given shell contains ions all of the same kind. Each shell has a characteristic angular dependence arising from the anisotropic hyperfine coupling. For rotation of the crystal about a [100] axis perpendicular to the external field [which places the external field in a (100) plane], shells 1 through 8 have the angular dependence shown in Figs. 3 through 9, respectively, where α is the angle between the external field and a [100] axis of the crystal lying in the plane perpendicular to the axis of rotation. Figure 10 shows the angular

dependence of the shell-2 nuclei for crystal rotation about a [110] axis perpendicular to the external field. Here α is the angle between the [110] direction in the plane perpendicular to the axis of rotation and H_0.

Within a given shell N, there are two sets of ENDOR lines arising from cases where the field of the electron at the nucleus either aids or opposes the external field. The two cases are called respectively "up" and "down." The separation of the "ups" and "downs" is equal to twice the Larmor frequency of the nuclei within the shell in the external field when the hyperfine interaction energy is greater than the nuclear Zeeman energy, and is equal to the hyperfine interaction energy when the nuclear Zeeman energy is greater. Thus the angular pattern for each shell appears twice. A study of this effect together with a study of the frequency of the ENDOR lines as a function of the magnitude of the external field allows identification of the kind of nuclei giving rise to the respective ENDOR lines. This with an angular study uniquely identifies the respective shells from the experimental data, except in those cases of shells having the same kind of nuclei and angular dependence. Among the first eight shells, this occurs only for shells 2 and 8. For this case shell 2 can be separated from shell 8 by the magnitude of the hyperfine interaction.
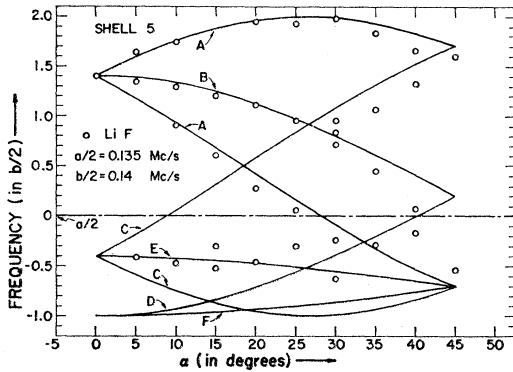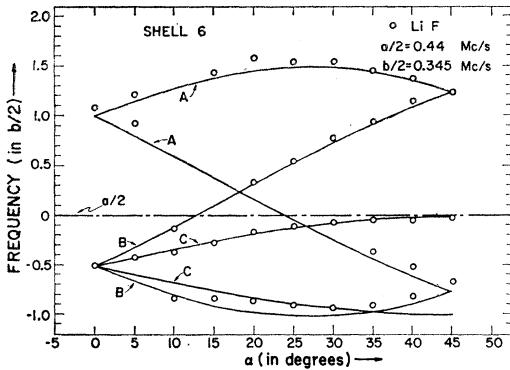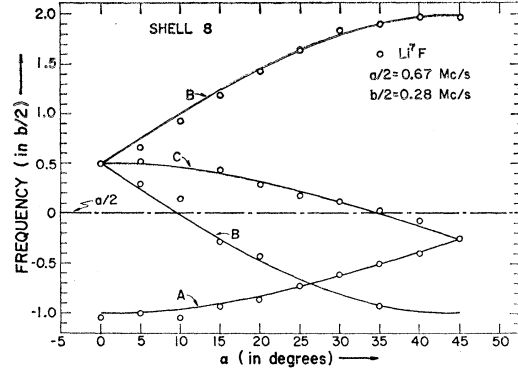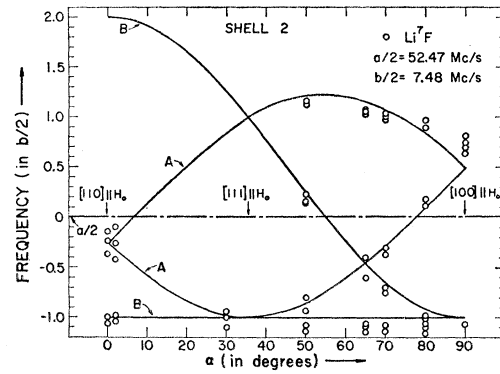

FIG. 7. Shell 5.

FIG. 8. Shell 6.

FIG. 9. Shell 8.

FIG. 10. Shell 2, [110] rotation axis.

The ENDOR pattern has thus far been computed using only first-order perturbation theory. Since each transition is degenerate, if the hyperfine coupling is treated to second order, subsidiary splittings of the lines arise. For the particular case of LiF F centers with the [100] crystal axis parallel to H_0, the second-order splittings arising from the 4 equivalent shell-2 fluorine nuclei located in the plane perpendicular to H_0 were observed. For this situation, the hyperfine interaction involving these four nuclei may be written

$$\mathcal{K}_{hf} = (a-b)S_z \sum_{k=1}^{4} I_{zk}$$

$$+[C(I_1^+ + I_3^+) + D(I_1^- + I_3^-) - C(I_2^+ + I_4^+)$$

$$+D(I_2^- + I_4^-)]S^+ + [D(I_1^+ + I_3^+)$$

$$+C(I_1^- + I_3^-) - C(I_2^- + I_4^-) + D(I_2^+ + I_4^+)]S^-, \quad (6)$$

where $C = \frac{3}{4}b$ and $D = \frac{1}{2}a + \frac{1}{4}b$. The four nuclei are in the xy-plane with the 1, 3 pair on the x axis and the 2, 4 pair on the y axis. The second-order perturbation may be performed separately on the electron spin operators. When this is done, a nuclear-spin Hamiltonian results, producing an effective nuclear-dipole dipole coupling. The proper basis functions of the nuclear states for evaluating this nuclear-spin Hamiltonian are those
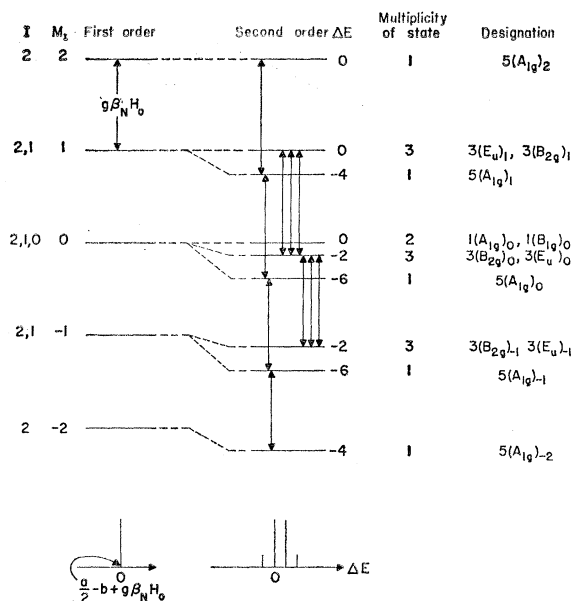
I	M_I	First order	Second order ΔE	Multiplicity of state	Designation
2	2		0	1	$5(A_{1g})_2$
2,1	1		0	3	$3(E_u)_1,\ 3(B_{2g})_1$
			-4	1	$5(A_{1g})_1$
2,1,0	0		0	2	$1(A_{1g})_0,\ 1(B_{1g})_0$
			-2	3	$3(B_{2g})_0,\ 3(E_u)_0$
			-6	1	$5(A_{1g})_0$
2,1	-1		-2	3	$3(B_{2g})_{-1}\ 3(E_u)_{-1}$
			-6	1	$5(A_{1g})_{-1}$
2	-2		-4	1	$5(A_{1g})_{-2}$

$g\beta_N H_0$

$\frac{a}{2}-b+g\beta_N H_0$ $\to \Delta E$

FIG. 11. Second-order hyperfine splitting, explained in the text. ΔE is in units of $a^2/4\nu_e$.

obeying the symmetry operations of the D_{4h} group.[27] The energy shift of each state (neglecting the aniso-tropic hyperfine coupling in second order), together with the $\Delta M_I = \pm 1$ transitions and the resulting spectrum for $M_S = +\frac{1}{2}$ are shown in Fig. 11. ΔE is given in units of $a^2/4\nu_e$, where ν_e is the microwave frequency. Relative intensities of the transitions are determined by the multiplicity of the energy states. The transition probabilities do not enter since the transitions are observed through the electron spin with the nuclear spin transition being saturated.

For the ENDOR technique to be successful, the relative magnitudes of the relaxation rates of the various relaxation mechanisms involved must be favorable.[28] It must be possible to saturate partially only a part of the inhomogeneous line. This implies that the effective spin-lattice time (T_1) is at least comparable to, if not shorter than, any time (T_{ss}) for spin diffusion through the line. The relative magnitudes of these two processes for a given set of experimental conditions determines the magnitude of the steady-state signal observed in dispersion while "hole eating" with field modulation applied.[29]

The ENDOR signals arise from spin population being transferred from some part of the inhomogeneous line into or out of the region where the "hole is eaten," thereby causing a momentary change in the amplitude of the steady-state microwave signal. This population transfer is produced by the applied rf field being swept

[27] H. M. McConnell, A. D. McLean, and C. A. Reilly, J. Chem. Phys. **23**, 1152 (1955).
[28] J. Lambe, N. Laurance, E. C. McIrvine, and R. W. Terhune, Phys. Rev. **122**, 1161 (1961).
[29] G. Feher, Phys. Rev. **114**, 1219 (1959).

in frequency in a fast passage manner through the frequencies corresponding to $\Delta M_I = \pm 1$ transitions for the neighboring nuclei. It is observed that the steady state and ENDOR signal intensities are a function of the orientation of the crystal in the external magnetic field, the largest steady-state and ENDOR signals (for shell-1 nuclei) occurring when a principle axis of the crystal is aligned parallel to H_0. The maximum ENDOR signal (shell-1 nuclei) does not always occur for "hole eating" at the center of the inhomogeneous line, but rather increases by as much as a factor of 2 to a maximum value on moving in either direction from the center. The steady-state signal is at maximum near the center of the resonance line. A plot of ENDOR signal amplitude and the steady-state signal amplitude as a function of H_0 for the shell-1 nuclei in LiCl F centers are shown in Fig. 12.

B. Slow Passage

In a slow passage experiment the external magnetic field with a low-amplitude field modulation super-imposed is slowly swept through the region where a low-intensity microwave field excites $\Delta M_S = \pm 1$ tran-sitions. Either the first or second derivative of the absorption line, depending on whether the fundamental or first harmonic of the field modulation frequency is phase detected, and the g value are thus obtained. If the over-all absorption line shape is nearly Gaussian, without appreciable structure, the root second moment may be obtained from a measurement of the center to peak of the experimentally obtained first derivative of the absorption curve. This can be compared directly to a second moment calculated from the Van Vleck expression,[30]

$$\langle \Delta H^2 \rangle = \tfrac{1}{3} \sum_\alpha a_\alpha'^2 I_\alpha (I_\alpha + 1), \qquad (7)$$

where a_α' is the effective hyperfine coupling constant for the α ion (isotropic and anisotropic). It is noted that a root second moment measurement cannot be used to obtain the hyperfine constants of shell 1.

The first derivative of the absorption curve may or may not show partially resolved structure, depending on the relative magnitude of the hyperfine coupling of the neighboring nuclei. Using the hyperfine constants obtained from ENDOR, the detailed shape of the absorption derivative may be calculated. The absorption spectrum to first order is given by

$$\Delta E_\alpha(M_i) = g\beta_0 H_0$$
$$+[a_\alpha + b_\alpha(3\cos^2\theta_\alpha - 1)]M_i(\text{shell}-1\text{ equiv.})$$
$$+[a_\alpha + b_\alpha(3\cos^2\theta_\alpha - 1)]M_i(\text{shell}-2\text{ equiv.}), \quad (8)$$

where M_i is the z component of the total spin of each group of equivalent ions in shells 1 and 2. Ions may be nonequivalent in first order either because of having different θ_α's for the particular orientation considered

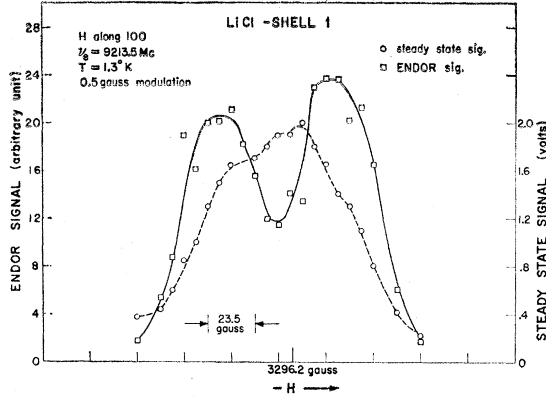[30] J. H. Van Vleck, Phys. Rev. **74**, 1168 (1948).

FIG. 12. ENDOR signal amplitude and steady-state signal amplitude as a function of H_0 for shell-1 nuclei in LiCl F centers.

or because of being a different isotope. The relative intensities of the transitions are given by the relative statistical weights of the different M_i levels. It is sufficient (because of the relative magnitude of the hyperfine constants) to include separately only the shell-1 and shell-2 ions. The effect of the remaining ion shells is included by using Eq. (7) to develop a root mean width of a Gaussian function, which is centered at each of the lines resulting from shells 1 and 2. The entire line shape is obtained by summing successively at each point of the line all of the contributions to the amplitude at that point.

Since the absorption line is symmetric about its center, a "measured" g value can be obtained. A "corrected" g value may then be calculated from the Breit-Rabi expression,[31]

$$g_{corr} = g_{meas} \left\{ 1 - \left\langle \sum_\alpha \frac{1}{2} \left(\frac{a_\alpha'}{H_0}\right)^2 [I_\alpha(I_\alpha+1) - M_\alpha^2] \right\rangle_{av} \right\}, \quad (9)$$

where H_0 is the field at the center of the absorption line, a_α' is the effective hyperfine coupling constant for the α ion (isotropic and anisotropic), and M_α is the quantum number of α ion. This correction is necessary since the experimental condition is not a high field situation where the hyperfine interaction energy is negligible compared to the Zeeman energy. A negative g shift from the free-electron g value occurs for the F center as is predicted from theoretical calculations which employ the spin-orbit interaction to produce this shift.

Equation (9) is correct when the linewidth is caused predominantly by a single shell of nuclei. Other cases are more complicated and call for a construction of the entire line with $a_\alpha'^2 M_\alpha^2$ taking on all its possible values with the proper weighting. The g shift is then found by observing where the center of the line now lies.

[31] G. Breit and I. Rabi, Phys. Rev. 38, 2082 (1931).

C. Fast Passage

In a fast passage experiment the external magnetic field is swept rapidly through the resonance in a time short compared to T_1 with a large microwave field incident on the sample. This is done with the spectrometer tuned to dispersion so that the signal received is proportional to the projection of the net magnetization along the microwave magnetic field at each instant. Thus, a picture is obtained of the difference in population between the $S_z = +\frac{1}{2}$, $I_z = +m$ to $-m$ and the $S_z = -\frac{1}{2}$, $I_z = +m$ to $-m$ energy levels, respectively, which existed before the passage through resonance. As a result of this passage, the populations of the $S_z = +\frac{1}{2}$, $I_z = +m$ to $-m$ levels are exchanged with the populations of the $S_z = -\frac{1}{2}$, $I_z = +m$ to $-m$ levels, respectively.

In the absence of a spin-spin relaxation process (T_{ss}), the conditions under which this phenomenon takes place are that the passage through the resonance is made in a time short compared to the spin-lattice relaxation time (T_1), and that $dH_0/dt < \gamma H_1^2$. If there is a spin-spin process, it will not be important as long as the passage through the line is short compared to T_{ss}. This situation is different from nuclear resonance where T_{ss} is comparable to the inverse line breadth, and inversion of the spin population can be achieved with fast-passage times long compared to T_{ss}. The observed fast-passage ESR line shape is given by[29]

$$M(H) = \pm M_0 \left(\frac{\ln 2}{\pi}\right)^{\frac{1}{2}} \frac{1}{\Delta H} \int_{-\infty}^{\infty} dH_i \left\{ \left(1 + \frac{(H_i - H)^2}{H_1^2}\right)^{-\frac{1}{2}} \right.$$

$$\left. \times \exp\left[-\ln 2 \left(\frac{H_i - H_0}{\Delta H}\right)^2\right] \right\}, \quad (10)$$

where H_1 is the magnitude of the microwave magnetic field, M_0 is the static magnetization, ΔH is the half-width at half-maximum of the line shape, and H_0 is the center of the resonance line. It is seen from Eq. (10) that the experimentally observed line shape is broadened by the effect of the finite H_1. When $H_1 < \Delta H$, this expression may be written[29]

$$M(H) = \pm M_0 (\ln 2/\pi)^{\frac{1}{2}} \exp(-x^2 \ln 2) (e^\beta) \left(\frac{H_1}{\Delta H}\right)$$

$$\times \left[\sum_{n=1}^{\infty} 2 \frac{(4\beta x^2 \ln 2)^n}{2^n} \frac{2^{n-1}(n-1)!}{(2n)! \beta^n} + K_0(\beta) \right], \quad (11)$$

where $x = (H - H_0)/\Delta H$, $\beta = (\frac{1}{2} \ln 2)(H_1/\Delta H)^2$, and K_0 is the zero-order Bessel function of the second kind.

The fast-passage technique may be used to measure T_1, and to detect the presence of any additional paramagnetic centers in the crystal. In order to measure the spin-lattice relaxation time, a sequence of pairs of fast passages through the resonance are made with different delay times between the two passages. In this
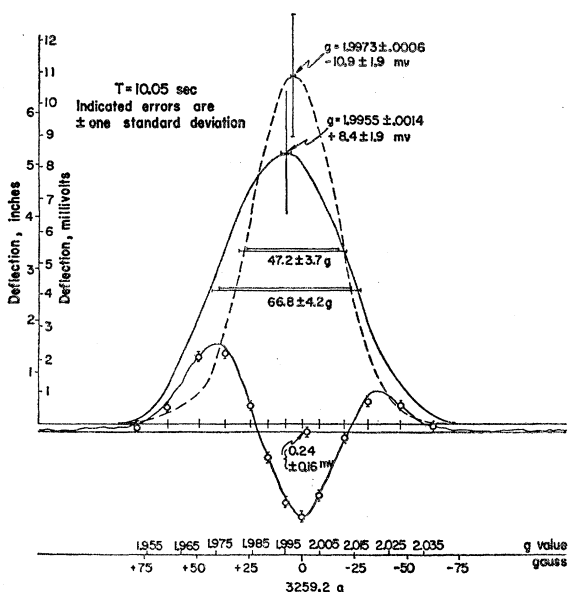
Fɪɢ. 13. Fast-passage KCl.

manner the second fast passage samples the distribution of spins among the energy levels while the spin system is recovering toward thermal equilibrium. Where a second paramagnetic center of low concentration and nearly the same g value and width is ordinarily obscured by the F center, it may be directly seen by this technique if the second fast passage through the resonances is made at a time when the energy levels connecting $\Delta M_s = \pm 1$ transitions belonging to the F center are equally populated. This description assumes that the Gaussian line shape of each center is fairly well preserved during relaxation and that the two centers are not coupled.

IV. EXPERIMENTAL PROCEDURE AND RESULTS

For each of the crystals investigated, the optical absorption spectrum and the three types of magnetic resonance spectra were observed. In many cases the optical density (OD) measurements showed the presence of color centers in addition to F centers. Likewise, additional magnetic resonance spectra were observed in the slow and fast passage experiments. However, no ENDOR lines were seen which could be attributed to additional paramagnetic centers. The additional resonances were not investigated except in the case of KCl.

A. Potassium Chloride

Additively colored KCl specimens were prepared by vacuum distillation of potassium into a Pyrex tube containing a KCl cube obtained from Harshaw, sealing the tube, and heating in an oven for 10 hr. During this time the crystal temperature was maintained at 600°C while the potassium temperature was varied from 150°C

to 400°C depending on the F-center concentration desired. At the conclusion of heating, the crystal was rapidly quenched to room temperature by sliding the tube directly from the oven into a paraffin oil bath, breaking the glass tube. Samples were then cleaved from the interior of the cube. All operations were done in illumination through a Wratten series 2 filter. Optical absorption measurements show only F centers present when the F-center concentration is less than $5\times10^{16}/\text{cm}^3$. Crystals containing from 5×10^{16} to greater than 10^{18} F centers/cm³ have M centers present.

Slow-passage measurements were made at 1.3°K and at 78°K on an additively colored KCl crystal which contained at least 10^{18} F centers/cm³ and had $\text{OD}_F/\text{OD}_M = 10$. With H_0 parallel to the [100] crystal axis, a single broad resonance line was seen with no resolved structure. The measured g value is 1.995 ± 0.002, and the root mean half-width is ~20 gauss. These values are in agreement with previously reported values ($g = 1.995\pm0.001$ and root mean half-width = 23 gauss).

ENDOR and fast-passage experiments were performed on numerous crystals which contained an F-center concentration from 10^{17} to greater than $10^{18}/\text{cm}^3$ and with the OD_F/OD_M ratio ranging from 10 to 2.5. The ENDOR experiments verified the results of Blumberg and Feher,[12] including the observation of a second-order hyperfine splitting and of lines arising from the 6.9% abundant K^{41} isotope. The nonaxially symmetric quadrupole splitting reported by Blumberg and Feher was not studied. No additional ENDOR lines were seen which might be attributed to a second paramagnetic center, even in samples where the optical absorption showed the presence of at least 10^{17} M centers/cm³ and where fast-passage measurements indicated the possible existence of a second paramagnetic center.

The results of the fast-passage measurements can be summarized by Fig. 13, which shows a typical second pass of a pair of fast passages made at 1.3°K. The experimental curve has been decomposed into two Gaussians by means of a least-squares analysis. The indicated full width at $\frac{1}{2}$-maximum of 66.8 ± 4.2 gauss [which is corrected to 49.5 ± 3.1 gauss peak to peak of the derivative for vanishing H_1 by Eq. (11)] and $g = 1.9955\pm0.0014$ for the broader slower relaxing center are in fair agreement with the accepted width and g value for the F center. The full width at $\frac{1}{2}$-maximum of 47.2 ± 3.7 gauss (which is corrected to 34.5 ± 2.7 gauss peak to peak of the derivative for vanishing H_1) and $g = 1.9973\pm0.0006$ of the second faster relaxing center are in the direction of the values reported by Kawamura and Ishiwatari for the M center[32] ($g = 2.00$ and peak to peak of the derivative $= 40.7$ gauss). However, no correlation between the amount of the second center present in the resonance

[32] H. Kawamura and K. Ishiwatari, J. Phys. Soc. Japan 13, 33 (1958).

TABLE I. Hyperfine constants.

Shell	Direction	Nucleus	Distance (A)	a (Mc/sec)	b (Mc/sec)	$A_\alpha|\psi_F(\alpha)|^2$ (cm$^{-3}\times10^{21}$)	$\langle(3\cos^2\theta_{\alpha F}-1)/r_{\alpha F}^3\rangle_{av}$ (cm$^{-5}\times10^{21}$)
				Sodium fluoride			
1	[100]	Na^{23}	2.31	105.6 ±0.8		603	
2	[110]	F^{19}	3.28	61.6		99	
3	[111]	Na^{23}	4.02	1.28±0.04	0.68±0.08	7.3	6.5
4	[200]	F^{19}	4.62	0.9 ±0.1	0.63±0.1	1.5	1.7
5	[210]	Na^{23}	5.18				
6	[211]	F^{19}	5.66	<0.94		<1.5	
8	[220]	F^{19}	6.55	0.9 ±0.04	0.65±0.02	1.5	1.8
				Sodium chloride			
1	[100]	Na^{23}	2.81	61.5±0.5	3.1 ±0.3	351	30
2	[110]	Cl^{35}	3.98	12.5 ±0.01	0.96±0.01	193	25
				Lithium fluoride			
1	[100]	Li^{7}	2.01	39.06±0.02 (GA=50)	3.20±0.01 (GA=2.8)	152 (GA=194) (Kojima=328)	21 (18)
2	[110]	F^{19}	2.85	105.94±0.02 (GA=61)	14.96±0.02	169 (GA=98) (Kojima=56.1)	40
3	[111]	Li^{7}	3.50	0.5 ±0.01 (GA=0.44)	0.68±0.02 (GA=0.72)	1.94 (GA=1.71)	4.43 (4.69)
4	[200]	F^{19}	4.02	0.48±0.01	1.12±0.01	0.77	3.01
5	[210]	Li^{7}	4.50	0.27±0.01	0.28±0.01	1.05	1.82
6	[211]	F^{19}	4.93	0.88±0.01	0.69±0.01	1.41	1.86
8	[220]	F^{19}	5.69	1.34±0.01	0.56±0.01	2.15	1.51
				Lithium chloride			
1	[100]	Li^{7}	2.57	19.1 ±0.1	1.72±0.06	74	11.2
2	[110]	Cl^{35}	3.66	11.24±0.15	0.90±0.05	173	23.3
3	[111]	Li^{7}	4.48	2.1 ±0.1	2.1 ±0.1	8.2	13.7
4	[200]	Cl^{35}	5.15	0.5	0.057	7.7	1.5
5	[210]	Li^{7}	5.75	<0.2		<0.78	
6	[211]	Cl^{35}	6.30	0.2	<0.03	3.1	0.8
8	[220]	Cl^{35}	7.28				
				Potassium chloride			
1	[100]	K^{39}	3.14	20.6	0.91	667	49.4
2	[110]	Cl^{35}	4.46	6.9	0.50	106.4	12.9
3	[111]	K^{39}	5.46	0.31	0.032	10.0	1.74
4	[200]	Cl^{35}	6.28	1.06	0.11	16.4	2.8
6	[211]	Cl^{35}	7.06	0.10	0.03	1.5	0.78
				Potassium bromide			
1	[100]	K^{39}	3.29	18.18±0.1	0.77±0.1	588.6	41.8
2	[110]	Br^{81}	4.65	42.2 ±0.2	2.4 ±0.2	236	22.5
4	[200]	Br^{81}	7.58	5.74±0.2	0.4 ±0.1	32.1	3.8

could be made with the M-center concentration, as determined from optical absorption measurements. The measured F-center relaxation time at 1.3°K ranged from 72 sec for 2×10^{17} F centers/cm³ to less than 3 sec for 10^{18} F centers/cm³ but depended on the previous history of the sample. For those crystals containing less than 5×10^{16} F centers/cm³ and containing no M centers as observed from the optical absorption spectra, the fast passage experiments showed the presence of only F centers with a relaxation time of 216 sec at 1.3°K.

Thus, the existence of a second paramagnetic center in crystals containing greater than 10^{17} F centers/cm³ is indicated since the observed second pass of the fast-passage pair is always asymmetric. It is unlikely that any "cross-relaxation" mechanism within a single center could produce this asymmetry. However, the origin of this resonance is not known.

B. Sodium Chloride

Sodium chloride crystals obtained from Harshaw were cleaved and exposed to 50-kv x rays for times ranging from 4 to 10 hours, producing an F-center density of at least 10^{18}/cm³ with $OD_F/OD_M=10$ as determined from optical absorption measurements. Slow-passage measurements at 1.3°K with the [100] crystal axis parallel to H_0 showed the F-center electron spin resonance unresolved with a g value slightly less than the free-electron g value and with the center to peak of the first derivative = 71 ± 10 gauss. Fast-passage studies gave a T_1 less than 3 sec.
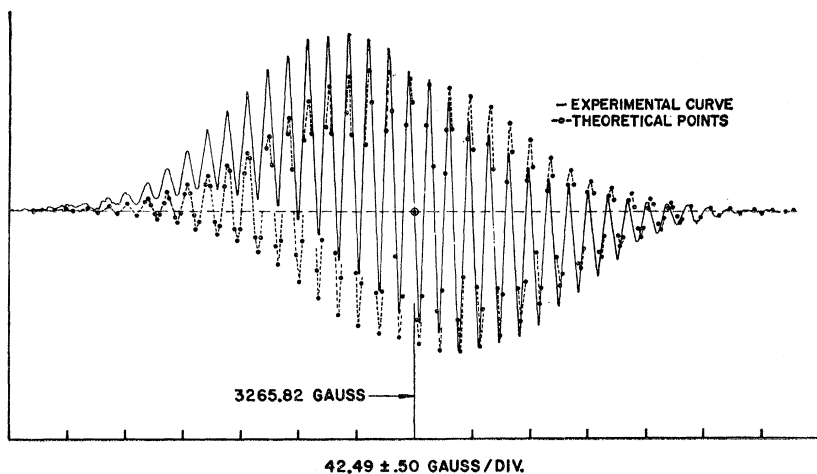
FIG. 14. LiF F-center spin resonance curve with [111] along H_0. Average line spacing$=14.7$ gauss.
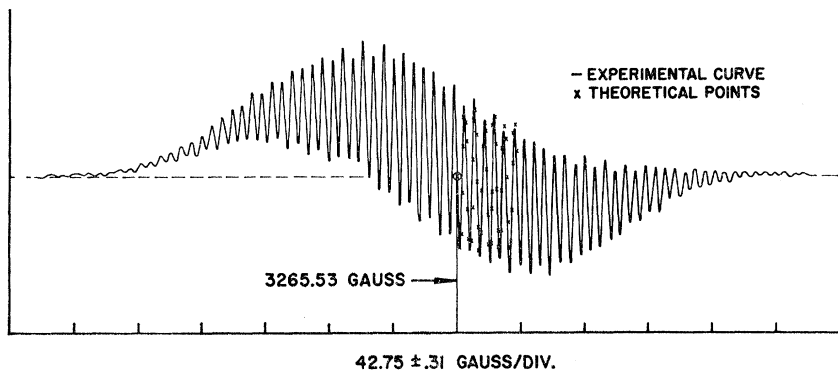
42.49 ±.50 GAUSS/DIV.

FIG. 15. LiF F-center spin resonance curve, 72° case. Average line spacing$=6.75$ gauss.

42.75 ±.31 GAUSS/DIV.

ENDOR experiments revealed the hyperfine coupling of the F electron to the two nearest shells of nuclei; the hyperfine constants are given in Table I. The quadrupole coupling appeared to be axially symmetric for the shell-2 nuclei with $Q'=0.1\pm0.02$ Mc/sec for Cl^{35}. The root second moment calculated from the measured hyperfine constants is 62.5 gauss, which is in rough agreement with the slow-passage value and is in agreement with Lord's value of 65.0 gauss.

C. Lithium Chloride

A single sample of LiCl, protected from the atmosphere since it is highly deliquescent, was exposed to 50-kv x rays for 20 hr. Optical density measurements showed an F-center concentration of at least $10^{18}/cm^3$, the F-band absorption peak at room temperature being at 385 mμ. The crystal was then sealed in the microwave cavity by partially filling the cavity with molten paraffin, which had been previously dried, and allowing it to solidify. All handling operations were done in a dry nitrogen atmosphere.

The slow-passage study at 1.3°K with H_0 parallel to the [100] crystal axis showed a single broad resonance with no resolved structure symmetric about $g=1.9970$ ±0.0008 with a measured center-to-peak of the first derivative$=28.6\pm4.0$ gauss. The integrated experimental curve is nearly Gaussian. The corresponding

resonance was seen in fast passage with $T_1=9.2$ sec at 1.3°K.

The hyperfine coupling to the neighboring nuclei was measured for nuclei through shell 8 in an ENDOR experiment; the hyperfine constants are given in Table I. A study was not made to determine whether or not the quadrupole splitting had axial symmetry. The quadrupole coupling constant for shell-2 nuclei is $Q=0.275$ Mc/sec for Cl^{35}. The root second moment calculated from the measured hyperfine constants is 24.3 gauss, which is in fair agreement with the slow-passage value.

D. Sodium Chloride

An NaF crystal obtained from Semi-Elements was cleaved and exposed to 50-kv x rays for 15 hr, producing at least 10^{18} F-centers/cm^3 with $OD_F/OD_M=5$. Slow-passage first derivative detection measurements made at 1.3°K with H_0 parallel to the [100] crystal axis showed the F-center resonance with a partially resolved structure consisting of 19 lines with a splitting of 37.7 ± 1.4 gauss, and with the resonance symmetric about $g_{meas}=2.0011\pm0.0008$. The lines were symmetric about the center of the resonance and decreased in amplitude from the center, although not uniformly. The center-to-peak of the first derivative curve was 110 ± 10 gauss which is in fair agreement with Lord's

FIG. 16. LiF F-center spin resonance curve with [100] along H_0. Average line spacing = 14.3 gauss.
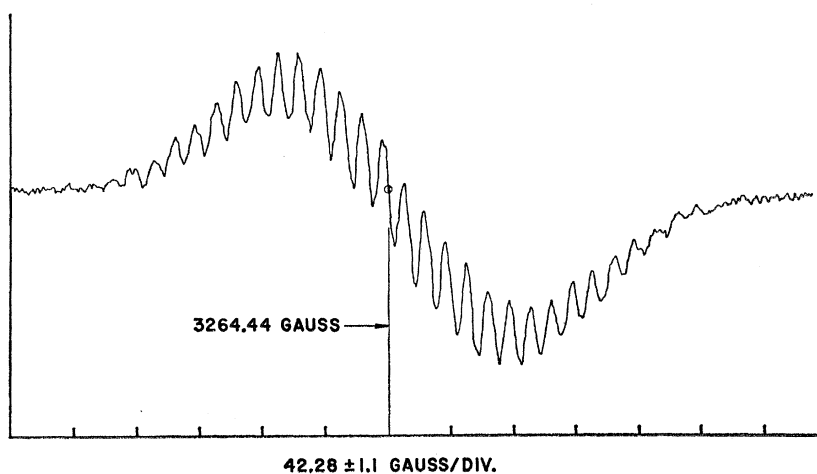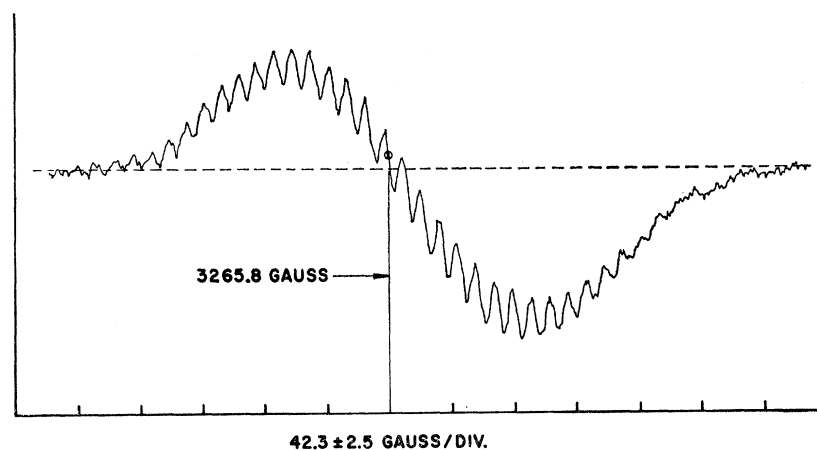
3264.44 GAUSS →

42.28 ± 1.1 GAUSS/DIV.

FIG. 17. LiF F-center spin resonance curve with [110] along H_0. Average line spacing = 12.1 gauss.

3265.8 GAUSS →

42.3 ± 2.5 GAUSS/DIV.

value of 104 gauss. An integral of the first derivative curve showed 17 partially resolved lines symmetric about the center. Slow-passage second derivative curves with H_0 parallel to the [100] and the [110] crystal axis showed in addition to the 19 main lines, 2 and 3 lines of lower intensity intermediate between each of the 19. Fast passage measurements reproduced the results of the integral of the first derivative slow passage curve.

ENDOR measurements showed the F-electron hyperfine coupling to nuclei of shells 3 through 8. The hyperfine constants for these shells are given in Table I. The F-electron hyperfine coupling to shells 1 and 2 was not seen. In the absence of complete ENDOR results, the interpretation of the second derivation slow-passage curve is not unique. The additional lines observed could arise from either a large anisotropic hyperfine coupling of the F electron to the shell-1 nuclei in which case the shell-1 b value would be $\frac{1}{10}$ of the shell-1 a value, or they could arise from a strong hyperfine coupling of the F electron to the shell-2 nuclei. In view of the evidence presented in the following section for LiF, it is felt that the latter possibility is the case. Thus, the assignment for those ENDOR lines

observed which had shells 2 and 8 symmetry was made to shell 8. The splitting of 37.7 gauss was taken for the shell-1 a value. The shell-2 a value was estimated from the shell-1 a value and the measured root second moment. These values are given in Table I.

E. Lithium Fluoride

F centers were produced in LiF crystals, which were obtained from Harshaw, by exposing the crystals at room temperature 50-kv x rays for times ranging from $\frac{1}{2}$ to 15 hr. The F-center concentration, as determined from optical absorption measurements, ranged from $10^{17}/cm^3$ to $10^{18}/cm^3$ while the OD_F/OD_M varied from 600 to 3.5, the larger M-center concentration occurring in the higher density F-center crystals.

Slow- and fast-passage resonance experiments at 1.3°K showed a broad Gaussian resonance line with partially resolved structure, the ratio of the structure amplitude to the broad curve amplitude and the spacing of the structure being dependent of the orientation of the crystal in the external magnetic field, as shown in Figs. 14–17. The measured $g = 2.0014 \pm 0.0006$ which is corrected to 2.0005 ± 0.0006.

The hyperfine constants of nuclei in shells 1 through 8 were obtained in an ENDOR experiment. The experimental points for shells 1 through 8 are shown, together with the theoretical curves, in Figs. 3 through 9, respectively. For these the [100] crystal axis is perpendicular to H_0, and is the axis of rotation; α is the angle between H_0 and a [100] crystal axis in the plane perpendicular to the rotation axis. Figure 10 shows the same comparison for shell-2 nuclei where the [110] crystal axis is perpendicular to H_0 and is the rotation axis. Here α is the angle between H_0 and the [110] axis in the plane perpendicular to the rotation axis.

Using these hyperfine constants, the slow-passage line shape has been calculated (using an IBM 704) by the method described in Sec. III for the [111] crystal axis parallel to H_0, and for the crystal aligned so that a line 72° from the [001] direction in the (110) plane is parallel to H_0. These calculations include the effects of the 7.43% abundant Li^6 isotope. A comparison of the calculated results with experiment is made in Figs. 14 and 15. It is noted that this calculation does not contain any adjustable parameters, and that the agreement is very good, verifying that the partially resolved structure observed arises from the F center.

F. Sodium Bromide

A piece of single-crystal Harshaw sodium bromide was cleaved in a dry nitrogen atmosphere, since it is slightly hygroscopic; then placed in a vacuum Dewar. It was then exposed to 50-kv x rays at room temperature for 20 hr. Optical density measurements showed an F-center concentration of more than 5×10^{17} F centers/cm³.

Slow-passage measurements at 1.3°K were made with H_0 along the [100] crystal axis. A broad Gaussian-shaped resonance was seen with $g_{meas} = 1.994 \pm 0.005$ and root second moment = 150.3 gauss. Fast-passage experiments yielded a single rather long relaxation time of 43 sec at 1.3°K.

ENDOR lines were not seen in the region from 1 to 80 Mc/sec.

G. Potassium Bromide

Potassium bromide single crystals, obtained from Harshaw, were additively colored and quenched from a high temperature in a mineral oil bath. All handling was done either in the dark or in illumination through a series 2 Wratten filter. The concentration of F centers determined from optical density measurements was greater than 1×10^{18}/cm³.

Slow-passage ESR experiments gave a g value of $g = 1.986 \pm 0.01$. The root second moment of the featureless Gaussian curve was 65 gauss. Fast-passage experiments were performed at 1.3°K but the relaxation time was less than 1 sec and could not be measured.

The hyperfine constants for those shells for which ENDOR lines were seen are given in Table I. The measured quadrupole coupling constants for shells 1 and 2 are, respectively, $Q' = 0.2 \pm 0.02$ Mc/sec and 0.25 ± 0.05 Mc/sec.

V. CONCLUSIONS

The ESR absorption line shape, with or without partially resolved structure, of F centers in alkali halides is completely explained as arising from the hyperfine coupling of the F electron to the neighboring nuclei. This has been accomplished by showing the agreement between the measured root second moment and that calculated from hyperfine constants obtained from ENDOR. The partially resolved structure existing on the ESR absorption derivative curve for F centers in LiF has been shown to arise from the hyperfine coupling by predicting the detailed shape of this curve from a calculation which employs the measured hyperfine constants. The deviation of the g values from the free-electron g value is always found to be negative. The previously reported positive g shift for LiF F centers, which implied a hole resonance, was remeasured and found to be negative.

The atomistic viewpoint of the F center adopted by Gourary and Adrian (GA) has been used by them in performing theoretical calculations on a number of different alkali halide crystals. GA perform a variational calculation with an F electron envelope wave function centered at the vacancy and a potential consisting of a lattice of point charges. This method is in contrast to the linear combination of atomic orbitals method employed by Kojima. Several forms of an F-electron envelope function have been tried by GA. They obtain their best ground-state energy when the F-electron envelope function (Ψ_F) has an S-type angular dependence and a radial dependence given by their type-III radial wave function, which is of the form $(1/r) \exp(-\eta r/a)$ outside the vacancy. This envelope function gives a reasonably good picture of the electronic charge distribution everywhere except in the immediate vicinity of the ions.

In hyperfine structure calculations, the detailed nature of the F-electron wave function at the ion cores is necessary. GA show that this function may be constructed by orthogonalizing the envelope function to the ion core orbitals. The problem is then one of calculating overlap integrals. Equation (12) is the GA approximated expression for the hyperfine coupling constant a_α, which relates the hyperfine constant to the product of $|\Psi_F|^2$ with an amplifying factor A_α.

$$a_\alpha = (16\pi/3)(\beta_0 \mu_\alpha / I_\alpha) A_\alpha |\Psi_F(\alpha)|^2. \qquad (12)$$

This equation is arrived at through the orthogonalization of Ψ_F to the core electrons of the α ion by the Schmidt orthogonalization procedure, where only the first nonvanishing term is kept in an expansion of Ψ_F about the α ion. Thus, $A_\alpha |\Psi_F|^2 = |\Phi|^2$ is the electron

density at the α nucleus. This procedure neglects overlap between ion core orbitals on different ions.

If Eq. (12) represents a reasonable approximation and if Ψ_F is an envelope function which varies smoothly from one crystal to another, then A_α will be dependent only on the core electrons of each particular kind of ion. It is interesting to present the results of ENDOR experiments in such a way as to compare the radial dependence of Ψ_F with experiment, demonstrate the dependence of A_α on ion position, and determine the validity of the approximation [Eq. (12)]. To accomplish

this, the experimental $|\Phi|^2$ values (the electron density at the α nucleus) are plotted together with theoretical $|\Psi_F|^2$ values (A_α is given an arbitrary value for this purpose) as a function of r for each crystal in Figs. 18 through 21. A_{exp} values are then determined by sliding the $|\Psi_F|^2$ curve on the semilog plot into correspondence with the near-neighbor experimental points of $|\Phi|^2$. This corresponds on the semilog plot to multiplication of $|\Psi_F|^2$ by a constant, A_{exp}.

It is seen from these figures that there is substantial agreement between theory and experiment in the radial
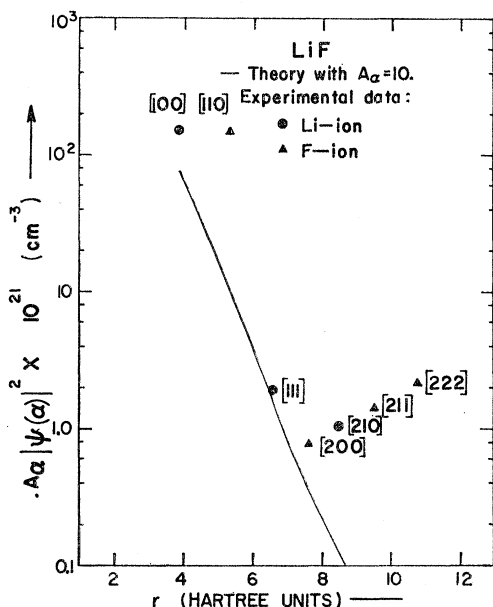

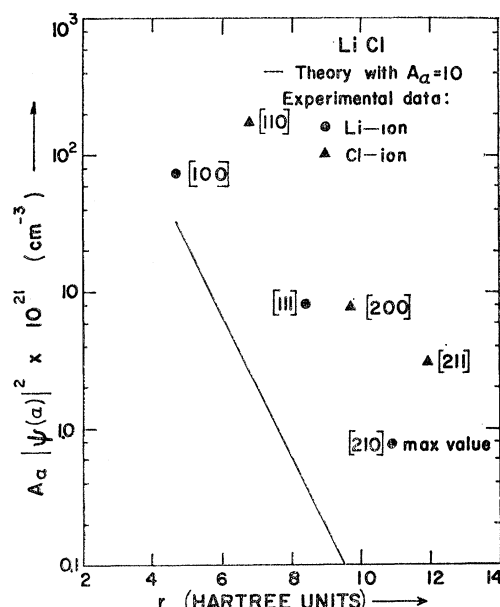FIG. 18. LiF isotropic radial dependence.

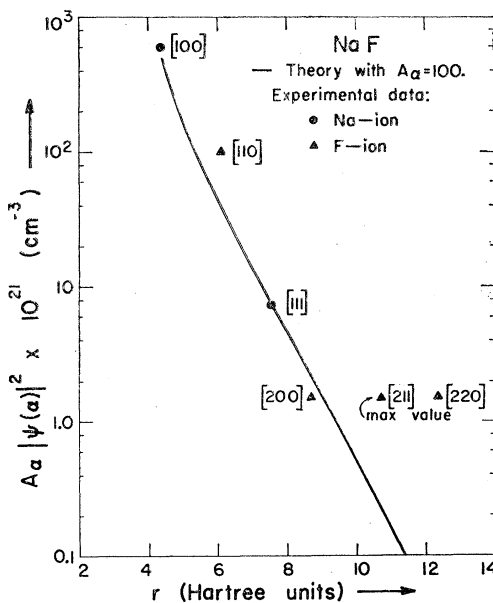FIG. 20. LiCl isotropic radial dependence.

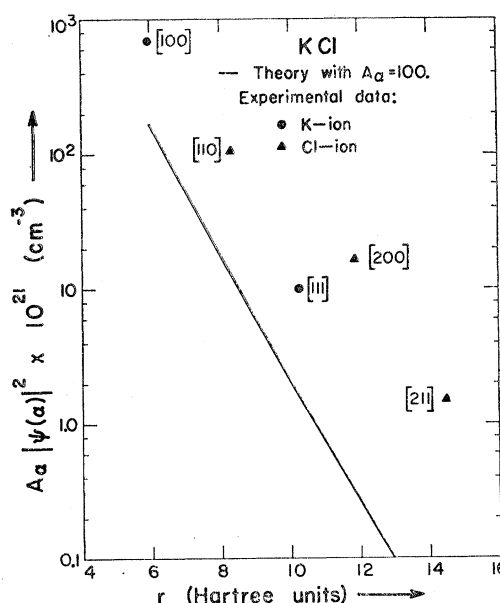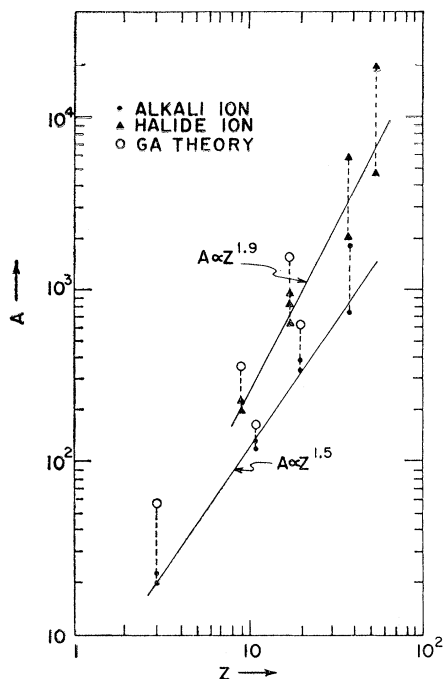FIG. 19. NaF isotropic radial dependence.

FIG. 21. KCl isotropic radial dependence.

FIG. 22. A value versus the atomic number (Z).

dependence of $|\Psi_F|^2$ with the A value being independent of the ion's location, except in the case of LiF and NaF where there are significant deviations in the outer ions. In these crystals, for the ions beyond shell 4, Eq. (1) is not as good an approximation since it neglects overlap between ion cores which one would

TABLE II. Experimental and theoretical A values.

Ion	Crystal	Experiment	$A_{exp.}$	A_{GA}
Li	LiF	ENDOR	20	57
Li	LiCl	ENDOR	22	⋯
Na	NaF	ENDOR	125	256
Na	NaCl	ENDOR	140	265
Na	NaBr	ESR	130[a]	⋯
K	HCl	ENDOR	381	640
K	KBr	ENDOR	333	⋯
K	KI	ESR	360[a]	⋯
Rb	RbCl	ESR	1800	⋯
Rb	RbBr	ESR	770	⋯
Rb	RbI	ESR	1290[a]	⋯
F	LiF	ENDOR	214	350
F	NaF	ENDOR	230	⋯
Cl	LiCl	ENDOR	637	⋯
Cl	NaCl	ENDOR	967	⋯
Cl	KCl	ENDOR	887	1500
Cl	RbCl	ESR	830[a]	⋯
Br	NaBr	ESR	5600	⋯
Br	KBr	ENDOR	1960	⋯
Br	RbBr	ESR	3800[a]	⋯
I	KI	ESR	4620	⋯
I	RbI	ESR	17500	⋯

[a] Denotes A value assumed to calculate opposing ion A value in crystal.

expect to be more important, especially for LiF which does not show clear ionic structure in x-ray spectra. In addition, the upward trend at the outer ions indicates the need of an angular dependence in Ψ_F such as a G function. Thus, in determining A_{exp} values for each ion in each crystal, only the first two neighbors of each kind of ion have been used. These A values, given in Table II, together with those determined by GA, are seen to be nearly independent of the particular crystal in which the ion is found. The GA A values are roughly twice the experimental A values. This point is discussed by Wood and Korringa.[33]

An average A value for each ion has been determined. Using these average A values, experimentally determined second moments, and estimates of the GA variational parameter (ξ) in those cases where GA do not state it, A values for the remainder of the alkali halides where ESR data are available have been determined. These results are only approximate. Experimental second moments are available for NaBr, RbBr, RbCl, RbI, and KI. In each case, as shown below, there are at least two measurements available on the same kind of ion in different crystals.

	Li	Na	K	Rb	
F	x	x			
Cl	x	x	x	$+$	(x indicates ENDOR)
Br		x	x	$+$	($+$indicates ESR)
I		$+$	$+$	$+$	

The A values for the Rb ion in RbCl and RbBr are determined from the known Cl-ion and Br-ion A values and the known RbCl and RbBr second moments, respectively. Likewise, the I-ion A value in KI is determined from the known K-ion A value and the known KI second moment. The I-ion A value in RbI is then determined from the previously determined Rb-ion A value and the known RbI second moment. These A values are given in Table II.

As shown in Fig. 22, a plot of these A values as a function of Z, the atomic number, shows that A is proportional to $Z^{1.5}$ and Z for alkali and halide ion, respectively. The GA A values (see Fig. 22) show similar dependence. The free atom hyperfine constants for the alkali atoms, with the dependence on the nuclear moment and spin removed $(A_{free\ atom})$, increase linearly with Z. If the correct description of the F center were given entirely by an LCAO method which neglected overlap, it would be expected that the $A_{F\ center}$ dependence on Z would be the same as the $A_{free\ atom}$ dependence. Thus, the GA point ion lattice and core orthogonalization methods appear to adequately describe the F center in general. The deviations of theory from experiment noted above are small corrections which are difficult to handle theoretically.

[33] R. F. Wood and J. Korringa, Phys. Rev. 123, 1138 (1961).

Drift Mobility of an Ionic Impurity in an Electric Field

John R. Manning

National Bureau of Standards, Washington, D. C.

(Received August 21, 1961)

When diffusion occurs by either a vacancy or interstitialcy mechanism, an electric field has two effects on the diffusion process. First, the field exerts a direct force on the electrically charged ions. This effectively changes the energy of motion for an ion jump in the direction of the field. Secondly, the field causes a net flow of vacancies or interstitialcies. This makes vacancies or interstitialcies approach an ion more frequently from one direction and less frequently from the opposite direction. The drift mobility μ of an ionic impurity in an electric field is found from consideration of these two effects, with μ being related to D^*, the tracer diffusion coefficient of the impurity in the absence of an electric field. General equations are derived giving the value of μ/D^* in any homogeneous cubic crystal. Explicit expressions are calculated for several specific lattices. These equations apply best when the impurity ion has the same charge as the solvent ions in the sublattice of interest. Both vacancy and interstitialcy mechanisms are treated. The value of μ/D^* depends on both the diffusion mechanism and the relative values of the various jump frequencies near the impurity.

1. INTRODUCTION

IN ionic crystals, ions diffuse by making a series of discrete jumps from one lattice site to another. The tracer diffusion coefficient D^* depends on the frequency of random jumps in all possible directions. An electric field will cause the ions to jump more frequently in one direction than another, and the drift mobility μ depends on this excess frequency of jumps. When the excess frequency is related to the random frequency, μ will be related to D^*.

In a homogeneous crystal, both μ and D^* can be determined from a single tracer experiment. If a layer of tracer ions on a plane normal to an electric field E is allowed to diffuse for a time τ, the center of the tracer profile will shift a distance $\bar{x} = \mu E \tau$ toward one end of the specimen. When E and τ are known, a measurement of the shift $\bar{x}$ allows one to calculate μ. The diffusion coefficient D^* can be found from the width of the tracer profile, which in a homogeneous crystal will be the same with or without a field.

In the present paper, results from a previous general treatment of diffusion in a gradient[1] are used to derive general expressions for μ/D^* in an electric field (electric potential gradient). Two separate contributions to the drift mobility are considered: (1) from the force the field exerts on the charged ions and (2) from the effect a flow of vacancies or interstitialcies has on the diffusion process. Expressions applicable to any homogeneous cubic crystal and to either a vacancy or interstitialcy mechanism are obtained. Explicit results for several common lattices then are calculated from these expressions. The nonrandom return of dissociating vacancies is considered, so, for self-diffusion, the equations are exact.

Relations between μ and D^* have been obtained previously in several special cases. If the ions pursue a random walk in the absence of an electric field, μ/D^* is given by the simple Nernst-Einstein relation,[2]

$$\mu/D^* = q/kT, \tag{1}$$

where q is the charge of the diffusing ions, k is Boltzmann's constant, and T is the absolute temperature. In general however, the ions will not follow a random walk. Thus, a correlation factor f must be introduced,[3] and Eq. (1) must be modified. McCombie and Lidiard[4] pointed out that, for self-diffusion, the value of μ depends on the total jump frequency ν, while the tracer diffusion coefficient D^* depends on the fre-

[1] J. R. Manning, Phys. Rev. 124, 470 (1961).

[2] See e.g., A. B. Lidiard, in *Handbuch der Physik*, edited by S. Flügge (Springer-Verlag, Berlin, 1957), Vol. 20, p. 324.

[3] J. Bardeen and C. Herring, in *Atom Movements* (American Society for Metals, Cleveland, Ohio, 1951), p. 87; also in *Imperfections in Nearly Perfect Crystals* (John Wiley & Sons, Inc., New York, 1952), p. 261.

[4] C. W. McCombie and A. B. Lidiard, Phys. Rev. 101, 1210 (1956).